AGU PUBLICATIONS

JGR

Journal of Geophysical Research: Solid Earth

RESEARCH ARTICLE
10.1002/2016JB013084

Key Points:
- In shear experiments the maximum principal stress triggers the quartz-to-coesite phase transformation
- Deformation enhances the transformation kinetics
- Pressures inferred from high-pressure phases in deformed rocks could overestimate the lithostatic pressure

Correspondence to:
B. Richter,
bettina.richter@unibas.ch

Citation:
Richter, B., H. Stünitz, and R. Heilbronner (2016), Stresses and pressures at the quartz-to-coesite phase transformation in shear deformation experiments, *J. Geophys. Res. Solid Earth*, *121*, doi:10.1002/2016JB013084.

Received 11 APR 2016
Accepted 6 NOV 2016
Accepted article online 9 NOV 2016

Stresses and pressures at the quartz-to-coesite phase transformation in shear deformation experiments

B. Richter[1], H. Stünitz[2,3], and R. Heilbronner[1,2]

[1]Geological Institute, Basel University, Basel, Switzerland, [2]Department of Geosciences, Tromsø University, Tromsø, Norway, [3]Institut des Sciences de la Terre d'Orléans, Université d'Orléans, Orléans, France

Abstract Coesite was found in quartz aggregates, experimentally deformed at confining pressures of 1.0–1.5 GPa and temperatures between 600°C and 900°C. The confining pressure (P_c) and, in most cases, the mean stress (σ_m) of the experiments were below those of the quartz-to-coesite phase transformation. Yet coesite formed when the maximum principal stress (σ_1) was within the *P-T* range of the coesite stability field. In one sample, the euhedral coesite grains were corroded indicating that coesite started to transform back to quartz. It is inferred that this sample started to deform with σ_1 above the quartz-to-coesite phase transformation and, with ongoing deformation, σ_1 decreased to values in the quartz stability field due to strain weakening. In all cases, σ_1 triggered the quartz-to-coesite reaction as well as the reverse reaction, suggesting that σ_1 is the critical parameter for the quartz-to-coesite transformation—not P_c or σ_m. With progressive deformation, the coesite laths rotated toward the shear plane as more rigid particles with the sense of shear. In case of back reaction, new quartz grains exhibit no systematic crystallographic relationship with respect to old coesite. The experiments cover different degrees of pressure "overstepping," different temperatures, and different experimental durations at *P* and *T*, and deformation always enhances the reaction kinetics. The observation that σ_1 is critical for a pressure-dependent phase transformation (also for reversals) poses questions for the thermodynamic treatment of such phase transformations.

1. Introduction

Since its discovery in natural rocks [*Chopin*, 1984; *Smith*, 1984], coesite, a high-pressure polymorph of silica, has been widely used as an indicator of high-pressure conditions in metamorphic rocks, because the phase transformation is only subordinately temperature dependent. Using piston cylinder apparatus, a number of studies have been carried out to establish the pressure and temperature conditions of the phase transformation [e.g., *Boyd and England*, 1960; *Kitahara and Kennedy*, 1964; *Mirwald and Massonne*, 1980; *Bohlen and Boettcher*, 1982; *Akella*, 1979; *Bose and Ganguly*, 1995]. A selection of transformation relations is shown in Figure 1. Several studies were dedicated to the kinetics of the phase transformation [e.g., *Mosenfelder and Bohlen*, 1997; *Perrillat et al.*, 2003; *Schönbohm*, 2003].

Using the experimental data by *Bohlen and Boettcher* [1982] and *Mirwald and Massonne* [1980] which are in good agreement at 800°C, *Akaogi et al.* [1995] were able to construct a consistent thermochemical database. Earlier, *Berman* [1988] also used the data of *Bohlen and Boettcher* [1982] to calculate the pressure, *P*, at the quartz-to-coesite phase transformation as a function of temperature. Following these two studies, we used $P\,(T) = 21.6 + 0.0079 \cdot T \pm 0.2$ (with pressure in kilobars and temperature in °C), the equation given by *Bohlen and Boettcher* [1982], as the most reliable one (see Figure 1). In the following, we will refer to *P* calculated from this *P-T* relation as the transformation pressure (see later).

In several deformation studies on quartz, performed in solid medium deformation apparatus, coesite was detected as a reaction product [e.g., *Hobbs*, 1968; *Green et al.*, 1970; *Hirth and Tullis*, 1994; *Zhou et al.*, 2005]. The reported applied confining pressures (P_c) were always considerably below the transformation pressure of the quartz-to-coesite phase transformation. *Green* [1972] explained the coesite formation by metastable growth from flint (partly amorphous SiO_2) according to the Ostwald step rule, while *Hirth and Tullis* [1994] attributed the formation of coesite to the effect of the maximum principal stress (σ_1) instead of the confining pressure.

The concept of (equilibrium) pressure, as used in thermodynamics, is based on the assumption of a (lithostatic) stress state, where all principal stresses are equal: $P = \sigma_1 = \sigma_2 = \sigma_3$. In absence of an equilibrium stress state, the mean stress σ_m (average principal stress, average *P*) is usually considered the equivalent of the

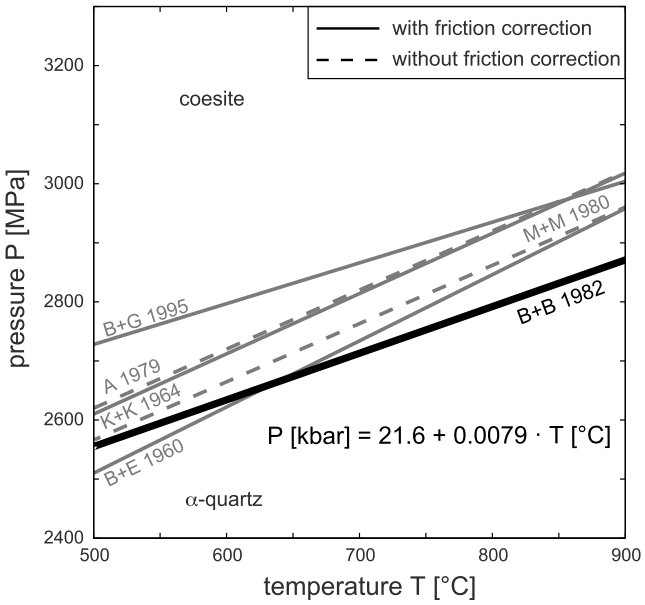

Figure 1. Selection of published *P-T* relations at the quartz-to-coesite phase transformation. Heavy line: B + B 1982—*Bohlen and Boettcher* [1982] (used in this study), *K* + K 1964—*Kitahara and Kennedy* [1964], B + E 1960—*Boyd and England* [1960], A 1979—*Akella* [1979], M + M 1980—*Mirwald and Massonne* [1980] (using α-quartz), B + G—*Bose and Ganguly* [1995].

pressure *P* [e.g., *Fitts*, 1962; *Stüwe and Sandiford*, 1994]. Under nonlithostatic stress conditions, the principal stresses are different and may have different effects on the metamorphic transformations depending on the specific processes that are involved, as discussed in several studies [e.g., *Kamb*, 1959; *Paterson*, 1973; *Shimizu*, 1992; *Wheeler*, 2014].

In polycrystalline rocks, stress raisers may exist, giving rise to local differential stresses, such that the normal stress acting on the grain boundaries could control reactions, e.g., pressure solution [e.g., *Shimizu*, 1992; *Wheeler*, 2014]. The interaction of stresses on grain boundaries and the consequences for pressure estimates were analyzed in recent studies [e.g., *Moulas et al*., 2013; *Wheeler*, 2014; *Tajčmanová et al.*, 2015; *Petrini and Podladchikov*, 2000]. *Wheeler* [2014] calculated the effect of differential stresses on the chemical potential along grain boundaries and showed that differential stress could significantly shift the pressure threshold for metamorphic reactions. *Moulas et al.* [2013] invoked a "pressure variation" (i.e., a differential stress) to which the rock as a whole is exposed. Their theory predicted that for equilibrium to exist after a phase transformation, the pressure of the new phase had to be close to the minimum or the maximum principal stress (σ_1 or σ_3). When considering observations made on experiments [e.g., *Hirth and Tullis*, 1994], they concluded that it should be σ_1.

Research on mineral equilibria under nonlithostatic stress is in its infancy and may require the application of nonhydrostatic thermodynamics. Such a treatment is beyond the scope of the study presented here. For the presentation and discussion of our experimental results, we will distinguish the following terms; in particular, we will refer to the (temperature dependent) pressure at the quartz-to-coesite transformation as the transformation pressure P_{trans} (1) principal stresses: σ_1, σ_2, and σ_3, where σ_1 is the maximum compressive stress; (2) confining pressure: P_c, in experiments $P_c = \sigma_3 = \sigma_2 < \sigma_1$; (3) mean stress: $\sigma_m = (\sigma_1 + \sigma_2 + \sigma_3)/3$, in experiments $\sigma_m = (\sigma_1 + 2P_c)/3$; (4) transformation pressure: P_{trans}, the pressure at the quartz-to-coesite transformation, as determined for a given temperature *T*; (5) σ_1-flow stress: the constant level of σ_1 during steady state deformation; (6) σ_1-overstepping: the amount by which σ_1 exceeds P_{trans} for the quartz-to-coesite transformation or the amount by which σ_1 falls below P_{trans} for the coesite-to-quartz transformation.

The kinetics of the coesite-to-quartz transformation has been studied to understand the preservation potential of coesite in high-pressure metamorphic rocks. The first-order reconstructive phase transformation between trigonal quartz and monoclinic coesite requires nucleation of a new phase and thus activation energy. Therefore, overstepping of the phase boundary has a strong effect on the kinetics of the phase transformation. As the quartz-to-coesite transformation is primarily pressure dependent, usually only pressure overstepping is considered, and overstepping of ~200 to 600 MPa has been applied in kinetic studies by *Mosenfelder and Bohlen* [1997] and *Perrillat et al.* [2003]. *Mosenfelder and Bohlen* [1997] found a strong dependence of the transformation on nucleation rate, while *Perrillat et al.* [2003] observed that nucleation rate was always fast, so that the growth rate was the controlling factor for the kinetics of the transformation. In addition, the growth rates of the coesite-to-quartz transformation reported by these studies differed by 1 order of magnitude or more.

Studies on the coesite-to-quartz transformation *published* so far are difficult to compare because the experimental procedures, the degree of overstepping, the grain size of the material, the water content, and the duration of the experiments vary considerably [*Mosenfelder and Bohlen*, 1997; *Perrillat et al*., 2003; *Schönbohm*, 2003]. *Mosenfelder and Bohlen* [1997] used single runs of loading and tried to minimize cracking during the preparation, whereas *Perrillat et al.* [2003] applied several cycles of prograde and retrograde transformations to one sample which may have increased the defect density in the material. This in turn could have caused higher nucleation rates as were indeed observed in the study by *Perrillat et al.* [2003].

All kinetic studies found that once a sufficient pressure overstepping was achieved, increasing the temperature had an additional enhancing effect on the rate of the phase transformation [*Mosenfelder and Bohlen*, 1997; *Perrillat et al*., 2003; *Schönbohm*, 2003]. *Perrillat et al.* [2003] observed lower transformation rates for the coesite-to-quartz transformation than the quartz-to-coesite transformation (by 1 order of magnitude). *Schönbohm* [2003] found significantly faster transformation rates for the coesite-to-quartz transformation than *Perrillat et al.* [2003], but the water content of the starting material in the study by *Perrillat et al.* [2003] was very small, while *Schönbohm* [2003] did not measure the exact water content (but high water contents were assumed).

In the study presented here coesite was formed in shear experiments performed on quartz aggregates in a modified Griggs apparatus at confining pressures below those of the phase transformation. In experiments where σ_1 exceeded the transformation pressure, coesite was found in the samples. Where σ_1 dropped below the transformation pressure again, the back reaction to quartz could be observed. We will discuss both the level of the principal stresses necessary to trigger the reaction and the influence of deformation and other parameters on the kinetics of the quartz-to-coesite phase transformation.

2. Experiments

Fifteen shear deformation experiments were carried out using two modified Griggs type solid medium deformation apparatus. The following sections address the preparation of the sample assembly, the experimental procedure, the description of the data processing, with special emphasis on the stress conditions, and the microstructural analysis methods.

2.1. Sample Preparation

The starting material was crushed quartz from a single crystal derived from a cleft in the Aar Massif (Planggenstock, Switzerland). Parts with few fluid inclusions were used. The inclusions were composed of H_2O-rich fluids with minor CO_2 and NaCl [*Tarantola et al*., 2012], but most of them decrepitated during the crushing procedure. All samples were prepared in the same way. A grain size fraction below 100 μm obtained by sieving was used. This powder, with 0.2 wt % H_2O added, was placed between 45° precut Al_2O_3 forcing blocks, where it formed a zone of ~1 mm thickness (Figure 2). This assembly was wrapped with a Ni foil and inserted into a Pt jacket, which was then weld sealed. The confining medium was solid NaCl. The temperature was controlled by S-type (Pt/Pt-Rh) or K-type (Cr-Al) thermocouples (depending on the deformation temperature). Maximum temperature fluctuations of ±3°C were recorded during experiments. The vertical temperature gradient inside the jacket was ~10°C mm^{-1} for experiments deformed at 700°C. A more detailed description of the sample assembly can be found in *Pec et al.* [2012a].

2.2. Experimental Procedure

The samples were pressurized and heated to the required deformation conditions within 5–9 h. The pressure was slowly increased to ~150 MPa, before heating the furnace to 100°C (heating rate 20°C min^{-1}), to prevent the added water from evaporating. Temperature and confining pressure were increased in alternating steps of 100°C and 100–200 MPa, respectively, such that the conditions always remained in the α-quartz stability field (Figure 3, inset). During pressurization the confining pressure (P_c) was nominally hydrostatic. A nonhydrostatic stress component on the samples (resulting from a difference between the load applied through the σ_1 and the σ_3 piston) could not be entirely avoided but rarely exceeded 100 MPa.

At the end of the pressurization, when the desired *P-T* conditions were reached (end of stage (1), Figure 3), the external pistons were in a piston-out position. The experiment was started by moving the σ_1 piston through the top lead piece to bring it into contact with the upper forcing block (see *Renner* [1996] for more

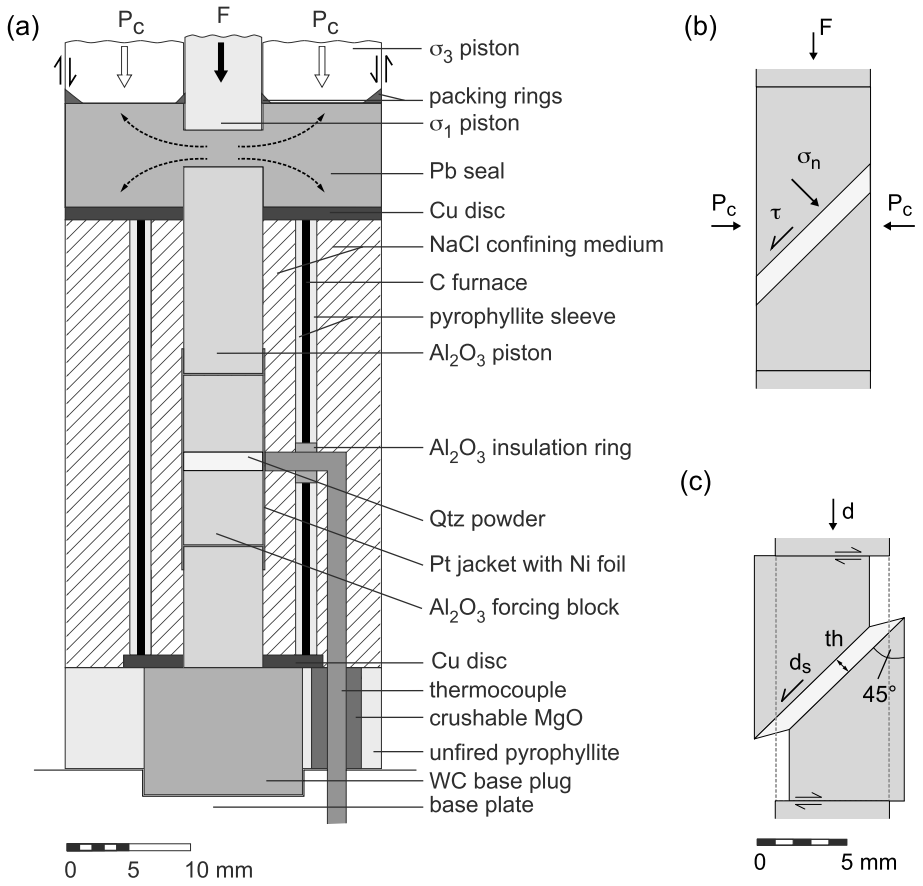

Figure 2. Sample assembly. (a) Sample (quartz powder) is inserted on 45° precut between forcing blocks, surrounded by the confining medium (NaCl) and a carbon furnace (modified after *Pec et al.* [2012a]). (b) Stresses in the sample: *F*—load applied to upper forcing block, P_c —confining pressure (MPa), σ_n—normal stress, τ—shear stress. (c) Sample geometry: *d*—displacement of σ_1 piston, th—thickness of sample, and d_s—shear displacement parallel to sample-forcing block interfaces. Small shear couple arrows indicate sideways escape of forcing blocks.

details). At the beginning of this so-called run-in (stage (2) in Figure 3) the load on the piston increased sharply by approximately 50–100 MPa (occasionally even more). After this, the force record curved over and increased gently throughout the run-in until it got close to the hit point where it started increasing again until it was as steep as the loading part of the force record (stage (3) in Figure 3). The hit point is therefore not well defined; rather, it has to be constructed. The "classical" hit point (point B, Figure 3) is obtained by intersecting the tangent lines to the run-in and the loading curve (dashed lines, Figure 3) as described, e.g., by *Pec* [2014]. In this study, we used point A (Figure 3) on the same tangent to the loading curve, however, at a load level that corresponds to the beginning of the run-in (obtained by intersecting the tangent lines to the initial steep part and the subsequent flatter part of the run-in stage).

After an initial steep increase of the load, the sample continued to deform at increasing, decreasing, or constant load levels. The experiment was stopped by quenching the sample to 200°C within 2 or 3 min (cooling rates 150–300°C min^{-1}) and retreating the σ_1 piston in such a way that σ_1 was at a slightly higher level (~200 MPa) than the confining pressure. The sample was depressurized to ~250 MPa followed by the decrease of pressure and temperature to room conditions.

2.3. Calculation of Stress and Strain in Sample

An external load cell was used to measure the force applied to the σ_1 piston (Figure 2a). A direct current displacement transducer (resolution ~1 μm) was used to record the displacement of the σ_1 piston relative to the steel frame of the Griggs apparatus; one of the machines (rig 2) was additionally equipped with a digital

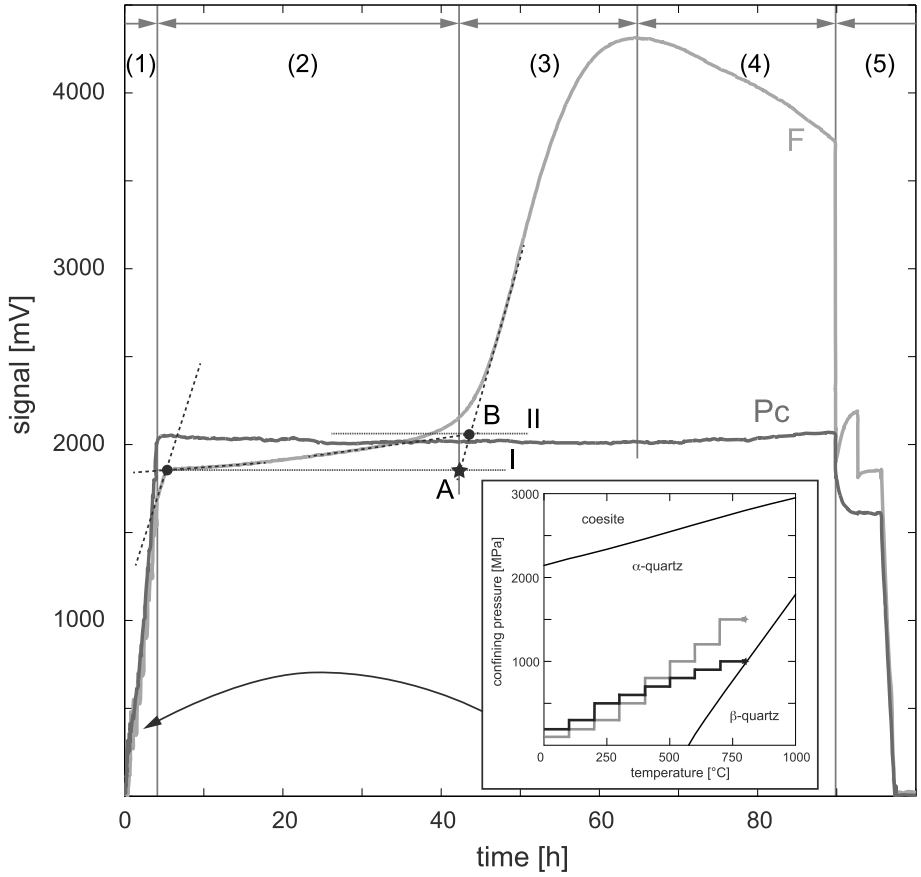

Figure 3. Signal-time plot of a typical mechanical data record (452br). *F*—force on σ_1 piston and P_c —confining pressure measured as oil pressure applied through the hydraulic ram. Five stages are indicated: (1) pressurization (static)—attaining *P-T* conditions, (2) run-in—advancing σ_1 piston through top lead piece, (3) loading of sample (4) deformation of sample, and (5) quenching and subsequent slow depressurization. The inset shows a schematic *P-T* path during pressurization for 800°C at 1.0 and 1.5 GPa in a SiO_2 phase diagram (calculated with Theriak Domino based on the Berman database, 1988; tridymite not shown).

linear-transformation measurement system (LTM, resolution = 0.1 μm). Measuring the pressure of the hydraulic ram, which actuates the σ_3 piston, continually monitored the confining pressure. All data were digitally recorded at a frequency of 1 Hz and analyzed with a modified version of one of the programs that were used previously [see, e.g., *Pec*, 2014]. The details of this correction are not the subject of this paper; however, the software can be downloaded from www.earth.unibas.ch/micro.

In a first step, the displacement, load, and pressure measurements were used to derive the principal stresses, σ_1 and σ_3, in the forcing blocks, which were assumed to remain undeformed under the applied *P*, *T*, and loading conditions. The second step was the calculation of the stresses transmitted to the deforming sample along the 45° precut.

Stresses in the forcing block: at the start of the experiment ($t = 0$), the minimum and the maximum principal stresses were both set to the value of the confining pressure measured at the hit point (A in Figure 3) such that $\sigma_1(0) = \sigma_3(0) = P_c$ and $\Delta\sigma(0) = 0.00$. The maximum principal stress (σ_1) was calculated by adding the differential stress ($\Delta\sigma$) to σ_3. During the experiment, σ_1(t) was calculated assuming a constant cross sectional area of the Al_2O_3 forcing blocks (Figure 2b), and $\Delta\sigma(t)$ was calculated as the difference between σ_1(t) and σ_3(t). It is assumed that σ_3 is not constant but increases with time as the σ_1 piston gets pushed into the pressure vessel.

The shear and normal stresses acting on the sample (across the piston sample interface) were calculated using the Mohr circle construction. For a sample orientated at 45° with respect to the applied σ_1, the shear stress $\tau(t) = \Delta\sigma(t)/2$, and the normal stress $\sigma_n(t) = (\sigma_1(t) + \sigma_3(t))/2$. Normal and shear stresses inside the sample

were calculated by balancing the normal and shear forces across the piston sample interface taking into consideration the ever decreasing area of piston overlap [*Heilbronner and Tullis*, 2006] and the increasing confining pressure [see *Heilbronner et al*., 2015] resulting in a combined correction for piston overlap and confining pressure buildup.

As the principal stress (σ_1) at $t = 0$ was not determined from the classical hit point but from the lower value of the new hit point (B in Figure 3), the so-called friction correction (an increase of σ_1 extrapolated from the slope of the run-in curve, see *Pec* [2014]) was not necessary. Also, the correction proposed by *Holyoke and Kronenberg* [2010] was not applied, as will be discussed later.

All samples thinned during the experiments, as could be measured after deformation. For the calculation of the shear strain ($\gamma = \mathrm{d}s/th$, see Figure 2), it was assumed that thinning was continuous and linear throughout the experiment. At each point, the shear strain was obtained by summing the incremental shear strains (calculated for decreasing sample thickness) between the recorded data points.

2.4. Texture and Microstructure Analysis

To analyze the microstructure, samples were cut parallel to the displacement direction and impregnated under vacuum with epoxy to prepare doubly polished thin sections. Thin sections were analyzed by means of light microscopy and scanning electron microscopy (Philips XL 30 ESEM). The acceleration voltage varied between 10 and 15 kV. Raman spectroscopy was conducted on a Bruker SENTERRA spectrometer using a 532 nm laser. For Electron backscatter diffraction (EBSD) analysis, the thin sections were polished additionally with colloidal silica suspension "OP-U-nondry" for 2 to 3 min. A field emission Zeiss Merlin scanning electron microscope (SEM) with a Nordlys nano camera was used, and the samples were analyzed in high vacuum. The data were acquired with Oxford AZtec software and processed with Channel 5 and MTEX. Grain sizes were calculated using the StripStar method [*Heilbronner and Barrett*, 2014].

3. Results

One suite of experiments was carried out at 1.5 GPa confining pressure and temperatures between 600°C and 900°C (Table 1). The shear strain rates varied between $\sim 2.5 \cdot 10^{-5}\,\mathrm{s}^{-1}$, $\sim 2.5 \cdot 10^{-4}\,\mathrm{s}^{-1}$ and $\sim 2.0 \cdot 10^{-3}\,\mathrm{s}^{-1}$. Additional experiments were conducted at 1.0 GPa confining pressure and temperatures of 650°C, 700°C, and 800°C.

3.1. Stresses, Pressures, and the Formation of Coesite

All samples were loaded to peak stress conditions and some were stopped at this point. Some samples displayed steady state or weakening stress conditions with ongoing deformation. Plotting the maximum principal stress (σ_1)—rather than the differential stress—against shear strain, the samples can be divided into three classes with respect to the quartz-to-coesite phase transformation (Figure 4):

1. The first class is characterized by the formation of coesite. In these experiments, σ_1 attained a level above the transformation pressure, P_{trans}, before reaching the peak stress and stayed above P_{trans} until quenching (Figure 4). Some experiments were stopped at or shortly after the peak stress yielding only small amounts of coesite.
2. In the second class, σ_1 never reached P_{trans} at any time during the entire experiment; no coesite could be detected.
3. In the third class (one experiment), σ_1 also reached a level above P_{trans} before reaching peak stress, and coesite was formed. As a consequence of strain weakening during the subsequent deformation, σ_1 fell below P_{trans} again (Figure 4a) triggering a reverse reaction of coesite to quartz.

This correlation between σ_1 and presence or absence of coesite is independent of confining pressure and shear strain rate. Whenever σ_1 exceeded P_{trans}, coesite was found in the samples, with the sole exception of experiment 338br, which was stopped close to peak stress. In it, no coesite could be found despite σ_1 having exceeded P_{trans}, suggesting that the duration of the experiment, in other words, transformation kinetics plays an important role.

In all of our experiments the confining pressure P_c and the mean stress σ_m stayed far below P_{trans} (Figures 5a and 5b). Data from published studies, also included in Figure 5, show a few cases where $\sigma_m > P_{\mathrm{trans}}$, due to the high

Journal of Geophysical Research: Solid Earth

10.1002/2016JB013084

Table 1. Experimental Conditions and Results

Experiment #	T (°C)	Pc (MPa)[a]	H_2O Content (μL)	Shear Strain Rate (10^{-5} s^{-1})	Shear Strain Y	Maximum σ_1 (MPa)[b]	Maximum $\Delta\sigma$ (MPa)[c]	Maximum σ_m[d]	σ_1 Overstepping (MPa)	Time (h)			Coesite
										Time at *P-T* Conditions	Deformation Time	Time in Coesite Field	
338br	600	1522	0.2	1.4	1.4	4042	2513	2367	1408	46.0	29.3	16.8	
479br	600	1538	0.2	2.1	3.9	4005	2423	2390	1370	72.2	57.1	43.9	<0.1%
435br[e]	650	1507	0.2	2.1	3.6	4242	2698	2449	1568	76.7	48.4	38.3	3.2%
481br[f]	650	1554	0.2	3.7	4.2	4085	2538	2393	1411	46.5	33.0	26.0	<0.5%
351br	700	1533	as is	2.7	2.6	2817	1247	1985	105	62.8	27.8	6.7	<0.1%
339br	700	1524	0.2	2.1	2.0	2837	1298	1971	124	50.2	27.5	6.5	<0.1%
437br	700	1529	0.2	1.9	1.7	3028	1483	2039	315	32.1	26.4	11.6	<0.5%
383br	700	1585	0.2	2.8	4.9	2808	1246	1987	95	97.6	50.3	17.3	1.9%[g]
388br	800	1527	0.2	2.8	4.8	2383	858	1813	-	69.0	49.8		
494br	650	1088	0.2	4.8	5.7	3547	2395	1950	913	49.8	34.7	23.9	<0.1%
452br	700	1064	0.2	2.7	4.4	2585	1535	1579	-	84.5	47.1		
448br	800	1067	0.2	2.9	4.5	1918	863	1347	-	69.3	44.2		
495br	750	1612	0.2	29	7.0	4098	2384	2509	1345	9.6	6.9	5.7	29.8%
447br	800	1556	0.2	27	4.1	3336	1783	2149	544	6.9	4.5	3.1	<0.5%
499br	900	1535	0.2	189	4.0	3597	2015	2255	726	1.1	0.6	0.4	<0.1%

[a]Mean confining pressure.
[b]Maximum principal stress $\sigma_1 = \sigma_3 + \Delta\sigma$.
[c]Differential stress $\Delta\sigma$.
[d]Mean stress $\sigma_m = 1/3\ (\sigma_1 + \sigma_3 + \sigma_3)$.
[e]Upper alumina piston deformed.
[f]Stick slip at the end.
[g]Back reaction of coesite to quartz indicated.

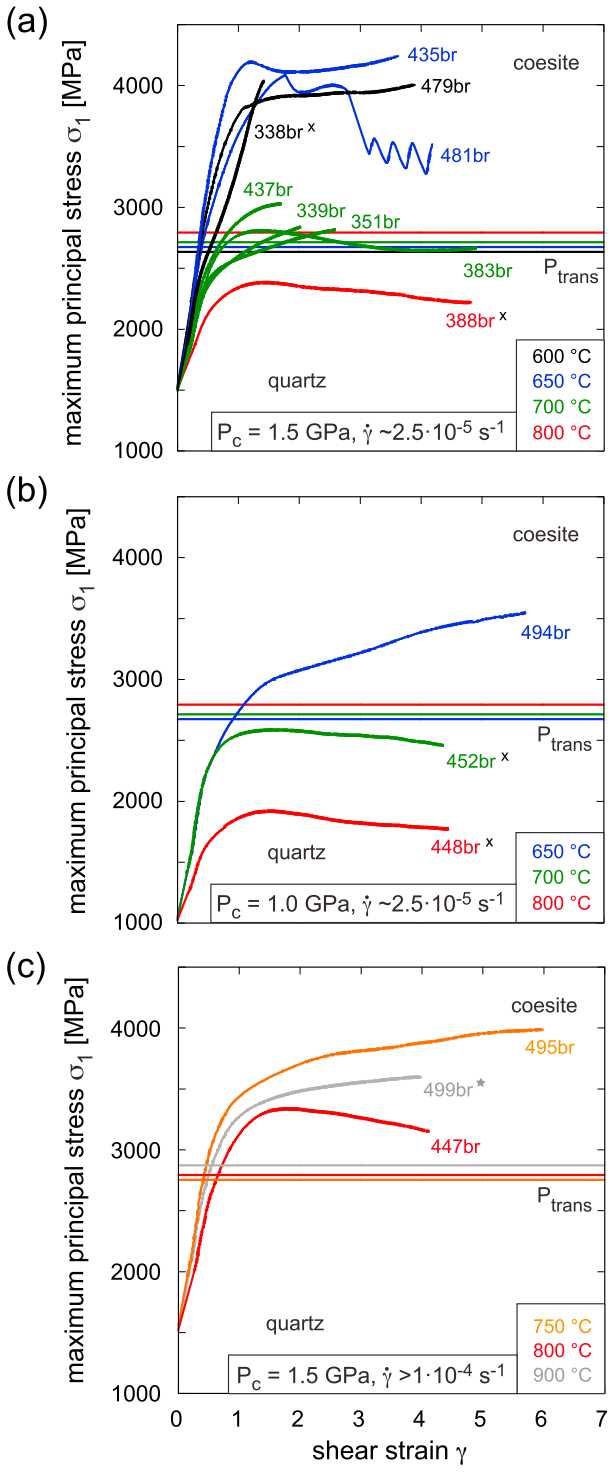

Figure 4. Maximum principal stress as a function of shear strain. The transformation pressure, P_{trans}, of the quartz-to-coesite phase transformation [after *Bohlen and Boettcher*, 1982] is marked by a horizontal line, color coded for each temperature. All samples, except those marked with a cross contain coesite. (a) Samples deformed at 1.5 GPa confining pressure and shear strain rates of ~$2.5 \cdot 10^{-5}$ s^{-1}. (b) Samples deformed at 1.0 GPa confining pressure and shear strain rates of ~$2.5 \cdot 10^{-5}$ s^{-1}. (c) Samples deformed at 1.5 GPa confining pressure and shear strain rates of ~$1 \cdot 10^{-4}$ s^{-1}. The star at 499br indicates an even faster strain rate of ~$1 \cdot 10^{-3}$ s^{-1}.

values reached for σ_1 [e.g., *Hirth and Tullis*, 1994]. In contrast, coesite formed if σ_1 exceeded P_{trans}, with one exception (338br) at 600°C (Figure 5c). If σ_1 stayed below P_{trans}, no coesite was found, even for values of σ_1 close to P_{trans}. The same correlation holds for the study by *Hirth and Tullis* [1994], with exceptions at low temperatures (500°C) where no coesite was detected despite σ_1 having exceeded P_{trans}.

3.2. Microstructural Observations of the Quartz-to-Coesite Phase Transformation

All samples start out as pure quartz powders and acquire, in the course of the experiments, typical dense quartz microstructures in response to compaction, temperature, flow stress, and strain rate. Coesite forms in a small volume fraction (see Table 1), and it probably does not influence the microstructure development of quartz in a significant way. Rather, coesite grains seem to nucleate and grow, adjusting to the deformation of quartz as rigid particles without deforming internally. In the next paragraphs, we therefore start by describing the microstructures and textures of quartz, followed by a description of coesite as well as the interaction between coesite and quartz.

3.2.1. Microstructure and Texture of Quartz

Samples deformed at 1.5 GPa and temperatures below 700°C are characterized by fracturing and probably frictional sliding, accompanied by dissolution-precipitation processes as well as the beginning of dynamic recrystallization. Riedel shears dominate the microstructure. At 700°C and higher temperatures, recrystallization becomes pervasive, and viscous deformation microstructures dominate. At low strain ($\gamma < 2$) or strain rates faster than 10^{-5} s^{-1}, shear bands develop. At high strains ($\gamma > 3$), samples are more homogeneously deformed with pervasive dynamic recrystallization (Figure 6).

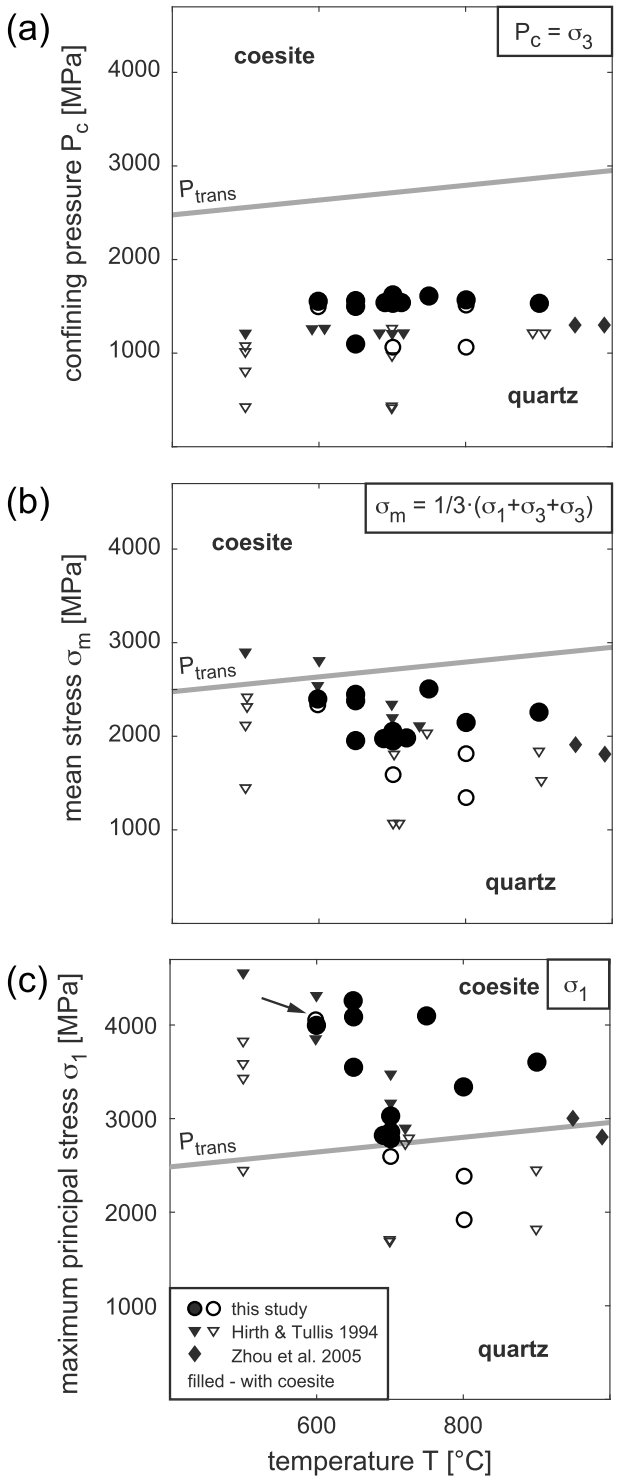

Figure 5. Pressure-temperature plots for maximum stresses reached during experiments. Data from present study and published data are compiled. Filled markers indicate coesite occurrence. P_{trans}—transformation pressure after *Bohlen and Boettcher* [1982] (line width proportional to an error of ±20 MPa). (a) Confining pressures ($P_c = \sigma_3$). (b) Mean stresses (σ_m). (c) Maximum principal stress (σ_1).

The recrystallized grains of the sample deformed at 700°C show a strong crystallographic preferred orientation (CPO) with one peripheral maximum of the *c* axes subnormal to the shear plane, rotated slightly with the sense of shear (red color coding of *Z* direction) and a maximum of *a* axes subparallel to the shearing direction (Figure 6a). The CPO is consistent with dislocation creep as the dominant deformation mechanism for quartz. The typical equivalent diameters of recrystallized grains in samples deformed at 700°C and 800°C (measured as the mode of the 3-D recalculated grain size distributions) are 2.5 μm and 5 μm, respectively. At lower temperatures or higher strain rates grains are smaller.

3.2.2. Microstructure and CPO of Coesite

Coesite crystals can be distinguished from quartz on account of their higher birefringence in light microscopy and higher *Z* contrast in SEM backscattered-electron (BSE) images (Figure 7). Using Raman spectroscopy, coesite is easily distinguished from quartz (Figure 8) by distinct peaks, at 465 cm^{-1} (quartz) and at 522 cm^{-1} (coesite). In measurements made in small grains both bands can appear. In this case, the signal is not considered as evidence for intergrowth between these two phases; rather, the Raman spectrum is a mixed signal of the small coesite grain and the surrounding quartz.

An elongated tabular shape characterizes euhedral coesite crystals with the largest diameter (less than 10 μm up to a few tens of micrometers) parallel to the *c* axis and the shortest diameter parallel to the *b* axis [*Renner et al.*, 2001]. Coesite grains (<20 μm largest diameter) appear around and between quartz clasts (diameter 30–40 μm, see Figure 7c), as well as dispersed among recrystallized grains. In highly deformed samples, the coesite platelets

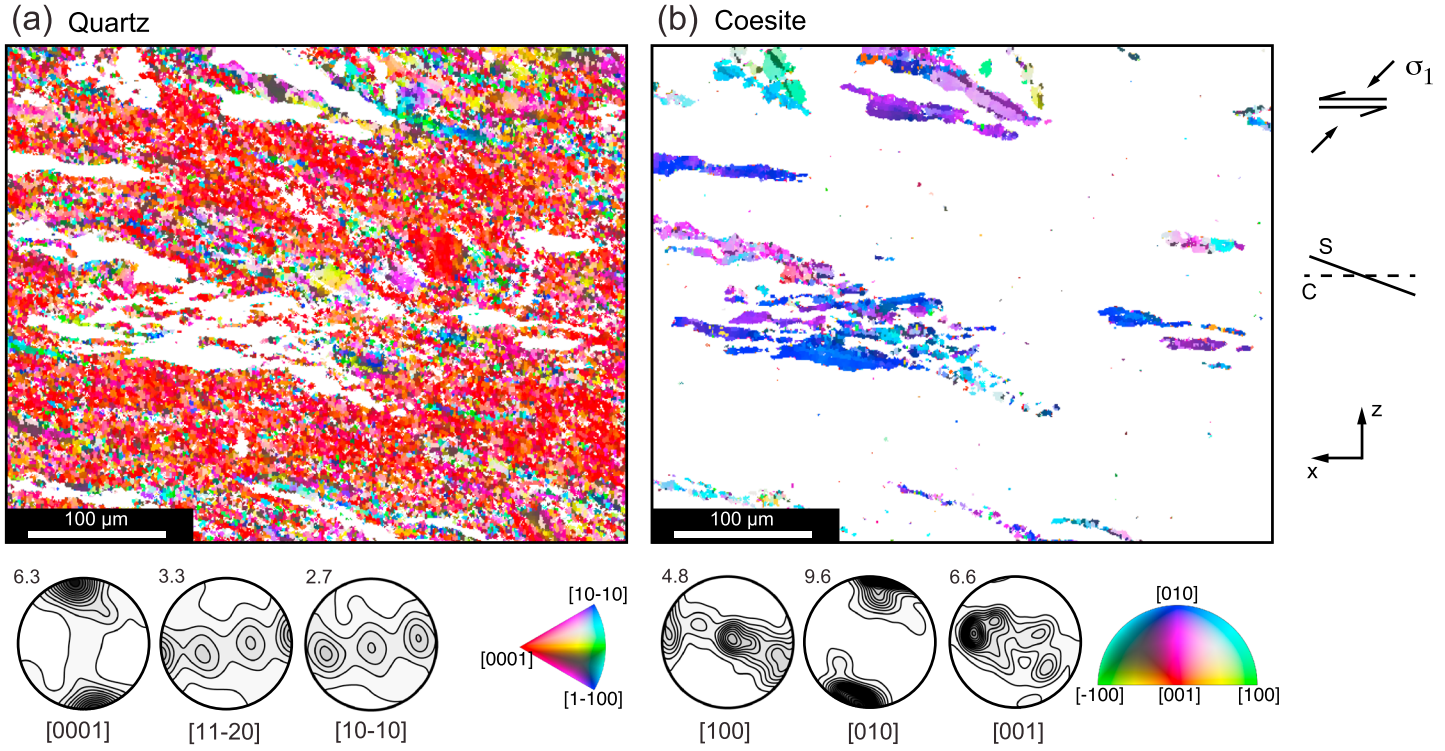

Figure 6. EBSD orientation maps of (a) quartz and (b) coesite. Sample 383br (step size 0.8 µm) with pole figures (maxima indicated, contour intervals 0.5 times uniform distribution), inverse pole figure color coding of *Z* direction (normal to shear plane).

(predominantly high aspect ratios > 2.5) are aligned at a small angle to the shear plane (Figures 7a and 6). Occasionally, multiple coesite grains seem to grow from single nucleation sites, forming rare spherulitic structures (Figure 7b). They may also grow from the surfaces of larger quartz grains (Figure 7c). In 383br (700°C, $\gamma \sim 5$), many coesite grains have partly lost their well-defined euhedral shape; instead, grain boundaries show a corroded appearance indicating the reverse transformation of coesite to quartz (Figures 7e and 7f).

In general, coesite forms throughout the sample, most abundantly in the region where the forcing blocks overlap (Figure 9). The less deformed end regions of the samples are always coesite free. Moreover, coesite is usually absent near the "heels" of the forcing blocks where stress concentrations are expected. In some cases, coesite may be related to local stress concentrations, for example, at contact surfaces of clasts (Figure 7c).

The amount of coesite found in the samples varies considerably. Three samples (435br, 383br, and 495br; Figure 9) deformed at 650°C, 700°C, and 750°C, respectively, show a distinct pattern. At 650°C, coesite crystals nucleate with random orientations at random sites within the quartz matrix as small volume fractions, often much less than 1 vol % (Table 1). At 700°C and with increasing shear deformation, the coesite platelets are rotated as rigid particles toward the shear plane in the dynamically recrystallizing quartz matrix. Volume fractions of 2–3 vol % coesite are attained. Finally, at 750°C, the volume fraction of coesite crystals keeps increasing (up to ~30 vol %) defining a wavy foliation (Figure 7a).

At high strain ($\gamma > 3$) and 700°C, coesite shows a strong CPO with a strong alignment of the {010} planes subparallel to the shear plane and the {100} planes subnormal to the shear plane (Figure 6b). The coesite grains do not display any dynamic recrystallization or bending of crystals (intracrystalline plasticity), so that the CPO is interpreted to be the consequence of the shape anisotropy and rotation of rigid tabular coesite grains toward the shear plane in the weaker quartz matrix.

Earlier studies indicate a growth relationship between coesite and quartz ([130]||[10–11], *Zinn*, 1996). This correlation could not be observed, neither for the growth of coesite on quartz nor for the reverse reaction. Furthermore, no clear growth direction of quartz on coesite was found.

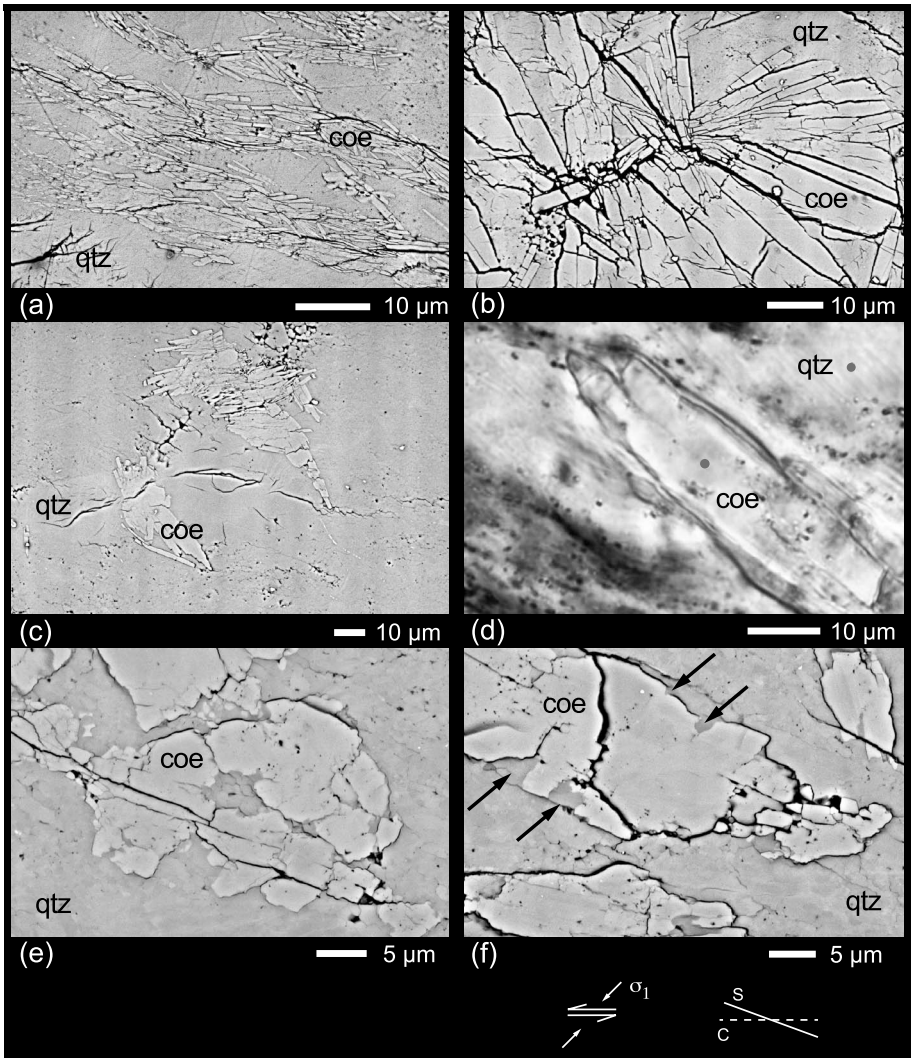

Figure 7. Coesite in deformed samples. (a) Alignment of coesite grains (495br, SEM/BSE). (b) Radial aggregate of coesite grains (435br, SEM/BSE). (c) Coesite grains nucleated along surface of quartz clasts (447br, SEM/BSE). (d) Single coesite grain embedded in quartz (383br, reflected light) with measurement points for Raman spectra (Figure 8). (e) Coesite grain with corroded appearance (383br, SEM/BSE). (f) Same as Figure 7e with arrows pointing to locations of the reverse coesite-to-quartz transformation.

3.2.3. Transformation Kinetics

A suite of experiments (339br, 351br, 383br, and 437br) performed at intermediate temperature of 700°C, 1.5 GPa, $10^{-5}\,s^{-1}$ and different amounts of finite strains ($2.0 < \gamma < 4.9$) shows that the longer the duration at the condition where $\sigma_1 > P_{trans}$ the more coesite forms (Figure 10). Samples 339br and 351br yield the same amount of coesite after 6.5 h and 6.7 h (<0.1 vol %) demonstrating good reproducibility. Sample 437br yields ~0.5 vol % after 11.6 h, and sample 383br yields ~1.9 vol % after 17.3 h. Note that 383br also shows microstructures of the reverse reaction of coesite to quartz; hence, the amount of coesite originally formed may have been slightly higher.

The lower the temperature, the more time is needed to obtain a given coesite fraction. For example, in sample 479br, deformed at 600°C and 43.9 h at $\sigma_1 > P_{trans}$, only a few coesite grains (<0.1 vol %) forms. In contrast, sample 435br, deformed at 650°C with 38.3 h at the same σ_1 overstepping and deformed at the same strain rate yields more than an order of magnitude more coesite (3.2 vol %; Figure 10 and Table 1).

The degree of σ_1 overstepping needs to be considered, too. High σ_1 overstepping during an experiment (~1350 to 1600 MPa, in 435br, 481br, 479br, 338br, and 495br) does not yield systematically higher amounts

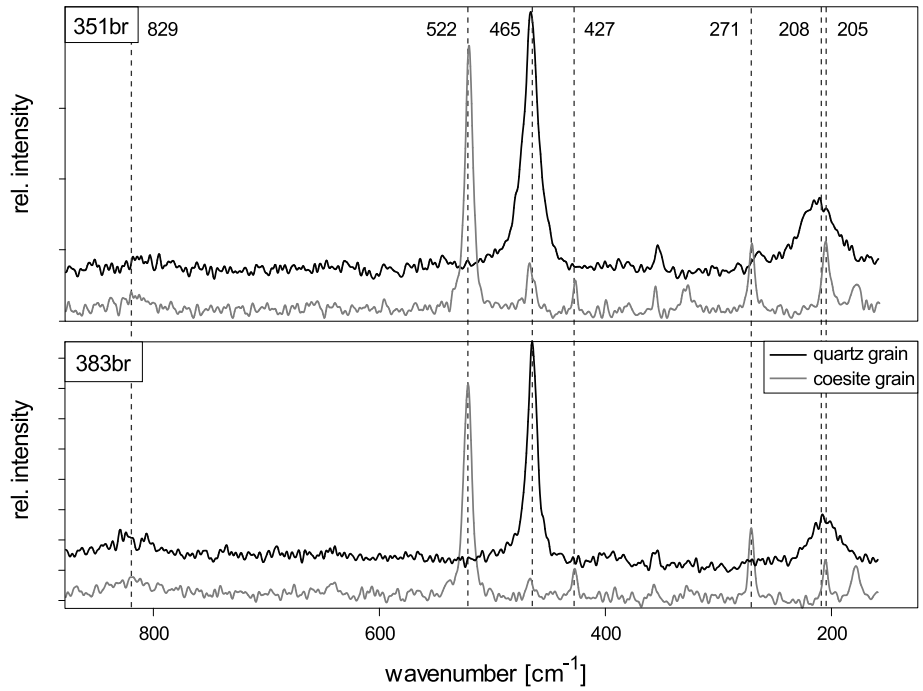

Figure 8. Raman spectra of quartz and coesite grains from two different samples. The small peak at 465 nm in the spectrum of the coesite grain of sample 351br is a background signal of the surrounding or underlying quartz. For wavelengths below 200 cm^{-1} the mineral spectra are superposed by epoxy in the thin section and therefore neglected. Spots of Raman measurements of sample 383br are marked in Figure 7d.

of coesite compared to lower σ_1 overstepping values (<500 MPa in 383br, 437br, and 447br)—temperature and strain rate are more important factors (Figure 10 and Table 1)

Despite the fact that the stress difference between σ_1 and P_{trans} and the time in the respective stability field was the same, the amount of quartz produced during the back transformation was very small. The precise amount could not be determined because we did not find a reliable criterion (textural or microstructural) that could help us distinguish between the back reacted and the original quartz in every case.

4. Discussion

The following discussion focuses on microstructural characteristics of the quartz-to-coesite phase transformation at nonhydrostatic stresses and the kinetics of this transformation. In addition, metastable formation and geological implications will be discussed.

4.1. Maximum Principal Stress as Critical Parameter for the Quartz-to-Coesite Phase Transformation

All coesite-bearing samples of our experiments were subjected to σ_1 higher than P_{trans} derived from nominally hydrostatic experiments (Figures 4 and 5). Samples without coesite experienced σ_1 below P_{trans}. At 700°C and $\gamma \sim 5$, the transformation from coesite back to quartz is observed. It is assumed that the back reaction starts when σ_1 decreases with progressive deformation and falls below P_{trans} (Figure 4a, sample no. 383br). The mean stress, σ_m, in samples containing coesite remains below P_{trans} (Figure 5b), even if the transformation pressures of *Bohlen and Boettcher* [1982] are used, the lowest of all experimentally determined pressures (Figure 1). The σ_m realized in our experiments cannot explain the coesite occurrence, because in most experiments, σ_m remains up to several hundreds of MPa below P_{trans}. Thus, using the mean stress concept as the representative for P_{trans} fails and it is implied that $\sigma_1 > P_{trans}$ is a sufficient condition for coesite formation.

The data set by *Hirth and Tullis* [1994] shows similar results as ours. All coesite-bearing samples experienced σ_1 higher than P_{trans}, but the mean stress of two coesite-bearing experiments by *Hirth and Tullis* [1994] reached P_{trans} for the given temperature (Figure 5b). Three samples deformed at 500°C had σ_1 values higher

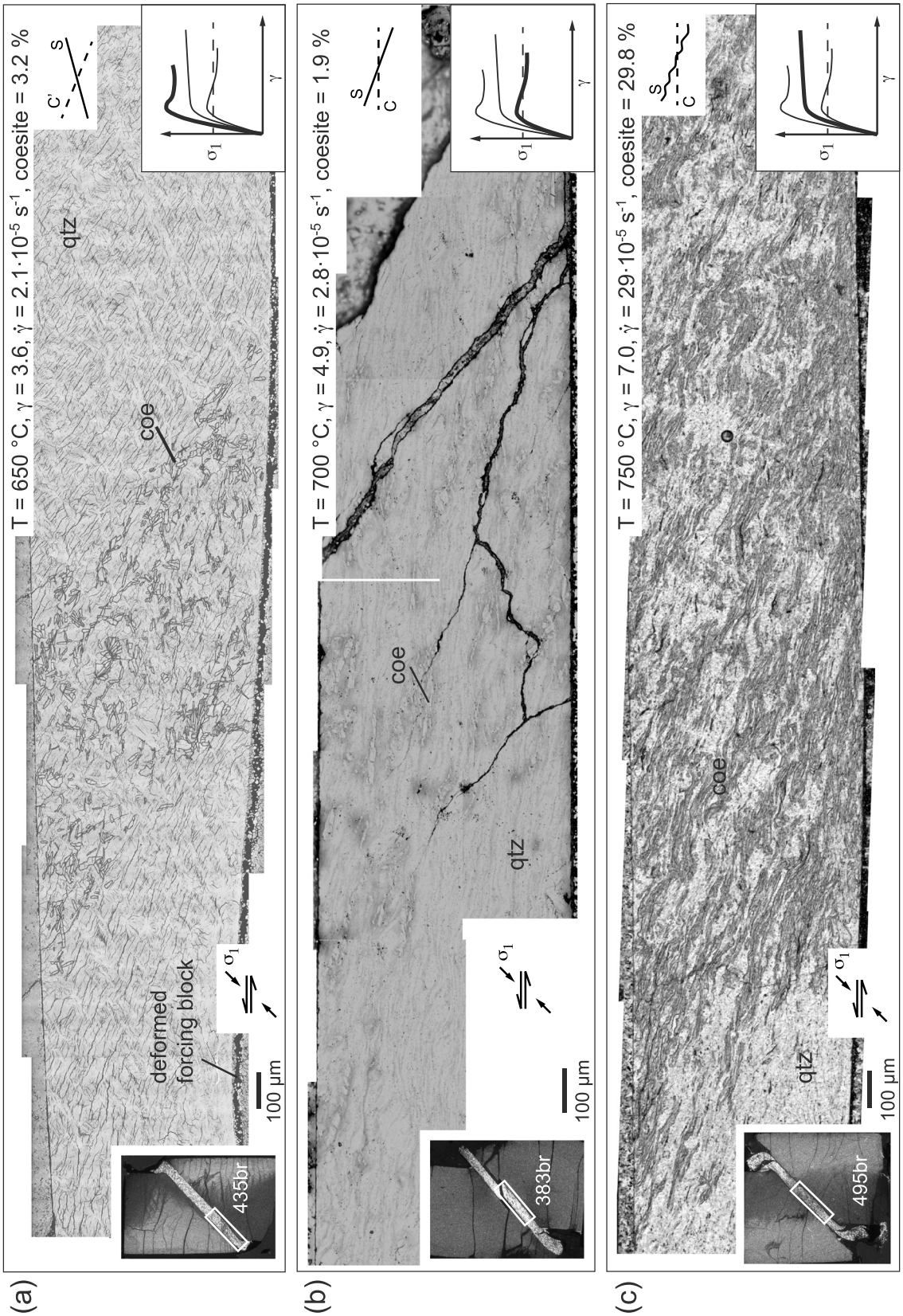

Figure 9. Distribution of coesite in samples after deformation. (a) Sample 435br (SEM/BSE image). Note deformed forcing block at left. (b) Sample 383br (reflected light with polarizer). (c) Sample 495br (transmitted light).

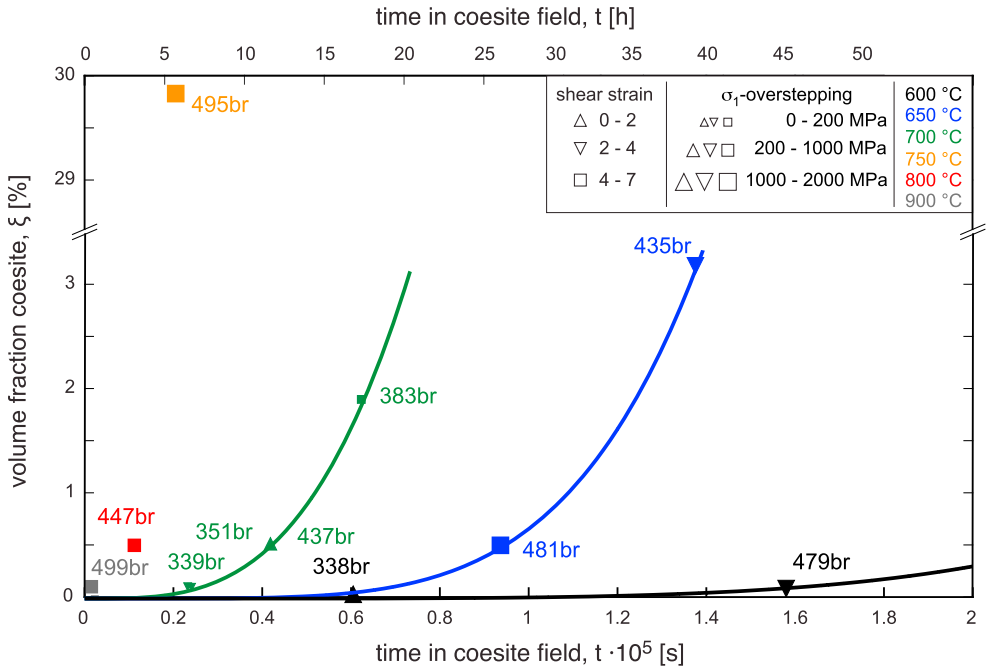

Figure 10. Avrami plot for coesite at 1.5 GPa confining pressure. Temperature is color coded, symbols denote amount of shear strain, and size of symbols denotes amount of σ_1 overstepping. Avrami equation is fitted to data at 700°C ($n = 3.3$ and $k = 4.8 \cdot 10^{-6}$), 650°C ($n = 4.9$ and $k = 3.6 \cdot 10^{-6}$), and 600°C ($n = 4.8$ and $k = 1.5 \cdot 10^{-6}$).

than P_{trans}, but no coesite was found (Figure 5c), which is most likely related to sluggish transformation kinetics at low temperatures. The study by *Zhou et al.* [2005] contains two coesite-bearing experiments where σ_1 values are close to P_{trans}. One experiment reached the coesite stability field, and the other one is in the quartz stability field, but in both of them coesite formed.

4.2. Metastable Formation of Coesite?

The σ_1 values in most samples of *Green* [1972] and one described in detail by *Hobbs* [1968] have remained below the P_{trans} of the quartz-to-coesite transformation, and only one of the two described samples of *Zhou et al.* [2005] has reached the P_{trans} without exceeding it (Figure 5). These situations are different from the ones described by *Hirth and Tullis* [1994] and those of this study, where in all coesite-containing samples σ_1 has been well above P_{trans}. Therefore, it is unlikely that in our samples coesite forms as a metastable phase as it is concluded by *Hobbs* [1968], *Green* [1972], and *Zhou et al.* [2005] for their experiments.

Furthermore, during deformation of all of our samples, a large part of the quartz recrystallizes dynamically. If coesite did form as a metastable phase, such coesite is expected to decompose (back transform) during continuing reconstitution (recrystallization) of the material. However, the back transformation of quartz to coesite is only observed in the sample, where σ_1 values decrease below P_{trans}. In addition, we do not observe a systematic effect of the confining pressure on coesite formation as inferred by *Zhou et al.* [2005]. Coesite occurs if the σ_1 values are higher than P_{trans}, at 1.0 GPa or 1.5 GPa confining pressure, P_c (i.e., σ_3) (see Figures 4a and 4b).

An extreme approach for the phase transformation in conjunction with deformation has been taken by *Su et al.* [2006], who ball milled their quartz samples before subjecting them to high pressure and temperature. Similar to *Kingma et al.* [1993], they observed the formation of an amorphous phase during ball milling and during subsequent high-pressure treatment; coesite grew after extremely short times (less than 1 min). Their results appear to be similar to those of *Green* [1972], who explained the formation of coesite below the transformation pressure as the result of metastable crystallization from partly amorphous material according to the Ostwald step rule. This rule implies that a metastable phase (coesite) nucleates and grows more efficiently than a stable phase (quartz) because the activation energy for the formation of the metastable phase with respect to the original material (partly amorphous SiO_2) is smaller than the activation energy for the stable

phase [*Green*, 1972]. The experiments of *Green et al.* [1970] and *Green* [1972] have been carried out using flint. Flint contains large amounts of amorphous silica, so that the Ostwald step rule applies to the formation of a crystalline phase from amorphous material. Our starting material consists of fully crystalline quartz, and no signs of amorphous material, produced during loading or deformation, have been observed. Furthermore, *Pec et al.* [2012b] produced (partly) amorphous material in experimentally deformed granitoid rocks where the quartz remained always crystalline and the amorphous domains are depleted in SiO_2 relative to the starting material, so that amorphization of quartz has never been observed. Given the reasons above, in our study, which considers the direct phase transformation from quartz to coesite, it is very unlikely that coesite should have formed as a metastable phase.

4.3. Effect of Potential Stress Raisers

Only bulk measurements of force can be made with our experimental equipment, and the stress states considered above refer to the entire sample. As the quartz powder is a polycrystalline material, the stress state of individual grains is expected to be heterogeneous and will depend on the neighborhood relationships, elastic anistropy, grain boundary orientations, etc. The analysis of the stress state of individual grains requires special equipment (see, e.g., *Bystricky et al.* [2015]—not commonly employed for hydrostatic and deformation experiments). The stress state of a grain boundary depends on the orientation of that boundary with respect to the acting forces. Therefore, the normal stress acting on a grain boundary was introduced as a scalar term by *Gibbs* [1906]. This approach was further developed by using the chemical potential to describe the stress state at grain boundaries [e.g., *Robin*, 1978] in the theory of pressure solution: For stress states with σ_1 above and σ_3 below the equilibrium pressure of the phase transformation, the high-pressure phase is expected to grow in the compression direction and react back to the low-pressure phase on the extensional side of the grains [*Shimizu*, 1992]. We do not observe a specific growth direction of coesite with respect to σ_1, probably because the more rigid character of coesite grains with respect to quartz causes an alignment of the coesite grains at a small angle to the shear plane during subsequent deformation stages (see Figures 6b, 7a, 9b, and 9c), so that the overall preferred orientation of coesite and, locally, its orientation with respect to the neighboring quartz is the result of this alignment rather than the original stress state.

Stress concentrations have to be expected in a polycrystalline material, especially when deforming in the brittle field. But in most samples we observe coesite distributed throughout the shear zone and not only in specific locations. Moreover, if stress raisers did occur, they should only persist for short time spans in a continuously deforming sample. If the stress concentration provided a stress high enough to nucleate coesite, the stress would decay instantaneously and coesite could not grow any further, because it is in a metastable state. Instead, the observed coesite of our samples indicates continued growth, and metastable growth has been excluded above. In samples that are dominated by brittle deformation processes (e.g., at low deformation temperatures and high strain rates) it is possible that stress raisers could persist. However, viscous deformation processes and extensive recrystallization (e.g., at high deformation temperatures) as occurred in our experiments make stress raisers an unlikely candidate for stable coesite formation.

4.4. Stress Estimates From Recorded Force Data

The force-displacement record of each experiment is converted to a stress-strain plot using the new combined correction for confining pressure and piston overlap. Both are a function of the advancement of the σ_1 piston and thus of the increasing shear strain. We did not use the stress correction proposed by *Holyoke and Kronenberg* [2010] because it was determined for coaxial experiments under low confining pressures ($\leq$0.4 GPa), while the experiments discussed here were performed under shearing conditions on quartz at high confining pressures (up to 1.5 GPa). Furthermore, the stresses published by *Hirth and Tullis* [1994] and *Zhou et al.* [2005], to which we compare our results (Figure 5), do not include this correction. Note that if the correction proposed by Holyoke and Kronenberg were used, the calculated maximum stresses of most of the coesite producing experiments shown in Figure 5 would not reach the coesite stability field.

In addition, sample 452br (700°C, 1.0 GPa confining pressure, $\gamma \sim 4.4$) remains below P_{trans} (~130 MPa) and does not contain any coesite, while 383br (700°C, 1.5 GPa confining pressure, $\gamma \sim 4.9$) exceeds P_{trans} by ~100 MPa and contains coesite. If the correction by *Holyoke and Kronenberg* [2010] would be applied, both samples would not reach P_{trans} and the absence or presence of coesite at these similar conditions (same temperature, similar shear strain and shear strain rate, difference in $\sigma_{1,max} < 230$ MPa) could not be explained.

4.5. Kinetics of the Quartz-to-Coesite Transformation

Our experiments were not originally intended for systematic kinetic studies of the quartz-to-coesite transformation, and systematic overstepping criteria are lacking. They were carried out with the aim of finding steady state flow stresses for quartz. Yet we can analyze semiquantitatively the transformation progress (expressed by the amount of coesite produced) that varies considerably with pressure overstepping, temperature, and strain [*Rubie and Thompson*, 1985] and fit an Avrami-type curve ($\xi = 1 - \exp(-(k \cdot t)^n$ with ξ (%)—volume fraction) to the amount of coesite formed (as vol %) against time spent in the coesite stability field (in seconds), (Figure 10). For $T = 700$°C our curve fit yields $n = 3.3$ and $k = 4.8 \cdot 10^{-6}$; for $T = 650$°C the curve yields $n = 4.9$ and $k = 3.6 \cdot 10^{-6}$; and for $T = 600$°C the curve yields $n = 4.8$ and $k = 1.5 \cdot 10^{-6}$. The increase of k with increasing temperature illustrates the temperature dependence of nucleation and growth rate, which are included in the k value [*Porter and Easterling*, 1992]. At 700°C, n is between 3 and 4, indicating the dominance of the nucleation rate. The high n values ($n > 4$) for lower temperatures can suggest an inhomogeneous distribution of nuclei or very high nucleation rates [*Sun et al*., 1996]. However, n values above 4 correlate with high overpressure (>1 GPa at 600°C and 650°C; see Table 1). Unfortunately, low volume fractions of coesite at 600°C make it difficult to fit the data.

For 700°C, 14.6 h are needed for the growth of 1 vol % coesite. In contrast after less than 1 s 1 vol % coesite has grown in *Perrillat et al.* [2003] experiments, which is faster than in our experiments. *Perrillat et al.* [2003] calculated n values below 1 ($n = 0.73 \pm 0.1$ for 700°C) indicating diffusion as controlling factor. The k values ($k = 2.3 \pm 0.5 \cdot 10^{-3}$ for 700°C) are higher by three orders of magnitude compared to our k values illustrating the earlier onset of the transformation. The H_2O content in our experiments is approximately 1 to 2 orders of magnitude higher than those of *Perrillat et al.* [2003]. A catalytic effect of H_2O on reaction kinetics is generally assumed, although its physical nature is not well understood. However, it should be noted that there are several parameters (e.g., grain size) that vary between our study and *Perrillat et al.* [2003]. The most important difference is the fact that we deformed our samples, and therefore, only σ_1 but not σ_m exceeds P_{trans} (i.e., in the coesite stability field). In contrast, static kinetic studies [e.g., *Perrillat et al*., 2003] have applied a constant pressure overstepping of σ_m.

The observations of different durations and extents of σ_1 overstepping, different finite strains, and different ξ values in samples deformed at 700°C (Figures 4 and 10) suggest that deformation and time spent in the coesite stability field have a greater kinetic effect on the transformation than the σ_1 overstepping alone. Furthermore, the back reaction has occurred to a small extent in 383br (Figure 7) even though the time is equal to the time in the coesite stability field, supporting the conclusion by *Perrillat et al.* [2003] that the coesite-to-quartz transformation is slower than the quartz-to-coesite one.

The slow reaction rates at low temperatures (≤600°C) appear to be the reason why coesite is not present in our sample 338br, although σ_1 exceeded P_{trans} by ~1400 MPa during ~17 h. In sample 479br (same temperature, confining pressure, σ_1 overstepping, and strain rate), which was in the coesite field for ~44 h, coesite is present (Figure 10), probably because the reaction rate is not fast enough at low temperatures of 600°C to form coesite at durations shorter than ~30–40 h. At 600°C and 650°C, σ_1 overstepping is similar (Figure 4), but the volume fraction of coesite is considerably higher after shorter duration (Figure 10). Probably the absence of coesite in the samples of *Hirth and Tullis* [1994], deformed at 500°C with high σ_1 overstepping values (Figure 5c), can be explained by the same kinetic barrier of low temperature.

In deformation experiments it is difficult to separate the quantitative contribution of individual factors to kinetics, such as temperature, strain rate, duration, and σ_1 or P_{trans} overstepping. It has been inferred for solid-solid metamorphic reactions between plagioclase and olivine that deformation may increase the reaction kinetics by approximately 1 order of magnitude [*De Ronde and Stünitz*, 2007]. As a consequence, it can be concluded that, in addition to temperature and pressure overstepping, deformation adds a third variable to the kinetics of the phase transformation.

The term "deformation" refers to the process and includes the effect of finite strain and strain rate. For example, samples deformed at high strain rates (Figure 4c) show the fastest reaction kinetics, i.e., the highest reaction rates of our samples in the Avrami plot (Figure 10 and Table 1). The deformation process will increase the Gibbs free energy (G) of the deforming phases, providing a driving potential for the transformation similar to overstepping [*Stünitz*, 1998; *De Ronde and Stünitz*, 2007]. It probably is not the dislocation density alone,

which provides the additional ΔG, because the dislocation density is proportional to the differential stress [*Kohlstedt*, 2007], and the differential stress in the high strain rate samples (495br, 499br, and 447br) has been similar to or lower than that of the lower strain rate samples (479br, 481br, and 338br), which show slower reaction kinetics (Figure 10 and Table 1). As the kinetics is strain rate dependent, it may be the energy dissipation rate during deformation [*Austin and Evans*, 2007], which plays an important role for the driving potential in reaction kinetics.

4.6. Geological Implication

The growth of coesite in these experiments illustrates that the high-pressure phase can nucleate and grow if σ_1 reaches values above P_{trans}, even if σ_3 or σ_m are below this pressure. Under low differential stresses, where the difference between σ_1 and σ_m is small, it is difficult to identify whether σ_1, σ_3, or σ_m is responsible for the phase transformation. Our results support the view expressed in the literature [e.g., *Schmalholz and Podladchikov*, 2014] that the presence of high-pressure phases in deformed rocks is not necessarily an indicator for high lithostatic pressure. Numerical models indicate the possibility of high differential stresses in parts of the lithosphere [*Schmalholz and Podladchikov*, 2013; *Reuber et al*., 2016]. The critical question is how high can differential stresses be in nature?

Typically, flow laws for wet quartz [*Paterson and Luan*, 1990; *Hirth et al*., 2001] indicate "normal" geological strain rates of 10^{-12} to 10^{-14} s^{-1} for differential stresses of tens to hundreds of MPa, so that these are typical estimates for natural conditions [e.g., *Wheeler*, 2014, and references therein]. Values of 300 ± 100 MPa have been independently determined for quartz, jadeite, and calcite at 300–350°C in *Küster and Stöckhert* [1999] and 50–100 MPa for dry quartz at ~800°C in *Menegon et al.* [2011]. In general, high σ_1 values are expected to occur in mechanically strong lithologies. Dry quartz has been proposed as an example for strong lithologies [e.g., *FitzGerald et al*., 2006; *Menegon et al*., 2011]. Therefore, dry quartz and a strong lithology at higher temperatures may be candidates for the occurrence of elevated differential stresses and thus phase transformation with σ_1 above P_{trans} and σ_m below P_{trans}.

Stress data are often "bulk" measurements on the kilometer scale. But there is evidence for local variations in the stress state (e.g., creeping fault segments) [*Rowe and Griffith*, 2015] if stresses localize over several decimeters to meters producing temporary stress raisers. In addition, the introduction of mechanically strong heterogenities in numerical models [*Reuber et al*., 2016] produces local high-stress regions in subduction zones, so that apparently, high σ_1 could be temporarily realized on a local scale. It should be noted that the stress raiser at the grain scale are transient in space and time. The mesoscopic stress raisers, mentioned above, could possibly be more persistent. Consequently, under high σ_1 new phases could grow, which normally are associated with higher depth. Therefore, depth estimates made from high-pressure phases in such situations could overestimate the actual depth.

Coesite is predominantly found as inclusions in mechanically strong phases, e.g., garnet, where the back reaction of coesite-to-quartz is suppressed [e.g., *Chopin*, 1984, 2003; *Tajčmanová et al*., 2015]. One of the main reasons given for the preservation is that the strong minerals may act as a "pressure vessel" and thus maintain a high pressure for the coesite [e.g., *Moulas et al*., 2013]. This study demonstrates that deformation enhances the reaction kinetics so that the back transformation of coesite to quartz is very likely to occur in a deforming matrix. So the back reaction to quartz may be likely—as in the case of a slowly deforming matrix (deformation active over a long time)—or impossible—as in the case where coesite may remain locked inside a nondeforming mineral.

5. Conclusions

In shear experiments, quartz can transform to coesite as soon as the maximum principal stress (σ_1) exceeds the (temperature dependent) pressure for transformation (P_{trans}) determined from hydrostatic experiments. The reverse transformation of coesite to quartz is triggered only when σ_1 drops below P_{trans} during strain weakening deformation. The formation of (stable) coesite can take place, even when P_c and σ_m are below P_{trans}; the formation of metastable coesite is excluded in our experiments.

The positive effect of the deformation process, namely, strain and strain rate, on the kinetics of the phase transformation can be separated qualitatively from the effect of temperature, time, and σ_1 overstepping. Enhancing effects of temperature, time, and σ_1 overstepping on kinetics are confirmed, too.

High maximum principal stresses (σ_1) associated with high differential stresses may induce phase transformations, such as quartz to coesite, at a shallower depth than equating lithostatic pressure and transformation pressure determined from isostatic experiments.

Acknowledgments

All data necessary to evaluate and build upon this work are included in the figures and tables; the data can also be obtained in electronic form by contacting the authors. We gratefully acknowledge the helpful discussions with Rüdiger Killian and Jiri Konopasek as well as the exchange with Evangelos Moulas, Lucie Tajčmanová, and John Wheeler. We thank the team of the centre of microscopy of the University of Basel for their assistance with the Philips XL 30 ESEM and Tom Ivar Eilertsen from Tromsø University for his assistance with the Zeiss Merlin SEM. Leander Franz is thanked for his help with the Raman spectrometer. Many thanks are due to Willy Tschudin for the excellent thin section preparation. Finally, the constructive reviews by two anonymous reviewers have improved the clarity of this paper and are greatly appreciated. Funding by the Swiss National Foundation grant NF200021-138216 is gratefully acknowledged.

References

Akaogi, M., H. Yusa, K. Shiraishi, and T. Suzuki (1995), Thermodynamic properties of α-quartz, coesite and stishovite and equilibrium phase relations at high pressures and temperatures, *J. Geophys. Res.*, *100*(22), 337–33,347, doi:10.1029/95JB02395.

Akella, J. (1979), Quartz-coesite transition and the comparative friction measurements in piston-cylinder apparatus using talc-alsimag-glass (TAG) and NaCl high-pressure cells, *Neues Jahrbuch für Mineralogie Monatshefte*, *5*, 217–224.

Austin, N. J., and B. Evans (2007), Paleowattmeters: A scaling relation for dynamically recrystallized grain size, *Geology*, *35*, 343–346, doi:10.1130/G23244A.1.

Berman, R. G. (1988), Internally-consistent thermodynamic data for minerals in the system Na_2O-K_2O-CaO-MgO-FeO-Fe_2O_3-Al_2O_3-SiO_2-TiO_2-H_2O-CO_2, *J. Petrol.*, *29*, 445–522, doi:10.1093/petrology/29.2.445.

Bohlen, S. R., and A. L. Boettcher (1982), The quartz-coesite transformation: A precise determination and the effects of other components, *J. Geophys. Res.*, *87*, 7073–7078, doi:10.1029/JB087iB08p07073.

Bose, K., and J. Ganguly (1995), Quartz-coesite transition revisited: Reversed experimental determination at 500-1200°C and retrieved thermochemical properties, *Am. Mineral.*, *80*, 231–238, doi:10.2138/am-1995-3-405.

Boyd, F. R., and J. L. England (1960), The quartz-coesite transition, *J. Geophys. Res.*, *65*, 749–756, doi:10.1029/JZ065i002p00749.

Bystricky, M., F. Béjina, and J. Baticle (2015), Effect of pressure on the deformation of forsterite and of iron-free enstatite, *Geotectonic Res.*, *97*, 126, doi:10.1127/1864-5658/2015-49.

Chopin, C. (1984), Coesite and pure pyrope in high-grade blueshists of the western Alps: A first record and some consequences, *Contrib. Mineral. Petrol.*, *86*, 107–118, doi:10.1007/BF00381838.

Chopin, C. (2003), Ultrahigh-pressure metamorphism: tracing continental crust into the mantle, *Earth Planet. Sci. Lett.*, *212*, 1–14, doi:10.1016/S0012-821X(03)00261-9.

De Ronde, A. A., and H. Stünitz (2007), Deformation-enhanced reaction in experimentally deformed plagioclase-olivine aggregates, *Contrib. Mineral. Petrol.*, *153*, 699–717, doi:10.1007/s00410-006-0171-7.

Fitts, D. (1962), *Nonequilibrium Thermodynamics*, pp. 173, McGraw-Hill, New York.

FitzGerald, J. D., N. S. Mancktelow, G. Pennacchioni, and K. Kunze (2006), Ultrafine-grained quartz mylonites from high-grade shear zones: Evidence for strong dry middle to lower crust, *Geology*, *34*, 369–372, doi:10.1130/G22099.1.

Gibbs, J. W. (1906), On the equilibrium of heterogeneous substances, in *The Scientific Papers of J. W. Gibbs*, vol. 1, Longmans, Green, and co., London.

Green, H. W., D. T. Griggs, and J. M. Christie (1970), Syntectonic and annealing recrystallisation of fine-grained quartz aggregates, in *Experimental and Natural Rock Deformation*, edited by P. Paulitsch, pp. 272–335, Springer, Berlin.

Green, H. W. (1972), Metastable growth of coesite in highly strained quartz, *J. Geophys. Res.*, *77*, 2478–2482, doi:10.1029/JB077i014p02478.

Heilbronner, R., and S. Barrett (2014), *Image Analysis in Earth Sciences*, pp. 520, Springer, Berlin.

Heilbronner, R., H. Stunitz, and B. Richter (2015), Calibrating the Grigg's apparatus using experiments performed at the quartz-coesite transition, paper presented at AGU fall meeting, San Francisco, Calif.

Heilbronner, R., and J. Tullis (2006), Evolution of c axis pole figures and grain size during dynamic recrystallization: Results from experimentally sheared quartzite, *J. Geophys. Res.*, *111*, B10202, doi:10.1029/2005JB004194.

Hirth, G., and J. Tullis (1994), The brittle-plastic transition in experimentally deformed quartz aggregates, *J. Geophys. Res.*, *99*, 11,731–11,747, doi:10.1029/93JB02873.

Hirth, G., C. Teyssie, and W. J. Dunlap (2001), An evoluation of quartzite flow laws based on comparisons between experimentally and naturally deformed rocks, *Int. J. Earth Sci.*, *90*, 77–87, doi:10.1007/s005310000152.

Hobbs, B. E. (1968), Recrystallization of single crystals of quartz, *Tectonophysics*, *6*, 353–401, doi:10.1016/0040-1951(68)90056-5.

Holyoke, C. W., III, and A. K. Kronenberg (2010), Accurate differential stress measurement using the molten salt cell and solid salt assemblies in the Griggs apparatus with applications to strength, piezometers and rheology, *Tectonophysics*, *494*, 17–31, doi:10.1016/j.tecto.2010.08.001.

Kamb, W. B. (1959), Theory of preferred crystal orientation developed by crystallization under stress, *J.Geol.*, *67*, 153–170.

Kingma, K. J., C. Meade, R. J. Hemley, H. Mao, and D. R. Veblen (1993), Microstructural Observations of α-Quartz Amorphization, *Science*, *259*, 666–669.

Kitahara, S., and G. C. Kennedy (1964), The quartz-coesite transition, *J. Geophys. Res.*, *69*(24), 5395–5400, doi:10.1029/JZ069i024p05395.

Kohlstedt, D. L. (2007), Properties of rocks and minerals—Constitutive equations, rheological behavior, and viscosity of rocks, in *Treatise on Geophysics*, vol. 2.14, edited by G. Schubert, pp. 389–417, Elsevier, Oxford.

Küster, M., and B. Stöckhert (1999), High differential stress and sublithostatic pore fluid pressure in the ductile regime-microstructural evidence for short-term post-seismic creep in the Sesia Zone, *Western Alps*, *Tectonophysics*, *303*, 263–277, doi:10.1016/S0040-1951(98)00256-X.

Menegon, L., P. Nasipuri, H. Stünitz, H. Behrens, and E. Ravna (2011), Dry and strong quartz during deformation of the lower crust in the presence of melt, *J. Geophys. Res.*, *116*, B10410, doi:10.1029/2011JB008371.

Mirwald, P. W., and H.-J. Massonne (1980), The low-high quartz and quartz-coesite transition to 40 kbar between 600° and 1600°C and some reconnaissance data on the effect of $NaAlO_2$ component on the low quartz-coesite transition, *J. Geophys. Res.*, *85*, 6983–6990, doi:10.1029/JB085iB12p06983.

Moulas, E., Y. Y. Podladchikov, L. Y. Aranovich, and D. Kostopoulos (2013), The problem of depth in geology: When pressure does not translate into depth, *Petrology*, *21*, 527–538, doi:10.1134/S0869591113060052.

Mosenfelder, J. L., and S. R. Bohlen (1997), Kinetics of the coesite to quartz transformation, *Earth Planet. Sci. Lett.*, *153*, 133–147, doi:10.1016/S0012-821X(97)00159-3.

Paterson, M. S. (1973), Nonhydrostatic thermodynamics and its geologic application, *Rev. Geophys. Space Phys.*, *11*(2), 355–389, doi:10.1029/RG011i002p00355.

Paterson, M. S., and F. C. Luan (1990), Quartzite rheology under geological conditions, in *Deformation, Rheology and Tectonics*, edited by R. J. Knipe and E. H. Rutter, *Geol. Soc. Spec. Publ.*, 54, 299–307, doi:10.1144/GSL.SP.1990.054.01.26.

Pec, M., H. Stünitz, and R. Heilbronner (2012a), Semi-brittle deformation of granitoid gouges in shear experiments at elevated pressures and temperatures, *J. Struct. Geol.*, *33*, 200–221, doi:10.1016/j.jsg.2011.09.001.

Pec, M., H. Stünitz, R. Heilbronner, M. Drury, and C. de Capitani (2012b), Origin of pseudotachylites in slow creep experiments, *Earth Planet. Sci. Lett.*, *355-356*, 299–310, doi:10.1016/j.epsl.2012.09.004.
Pec, M. (2014), Experimental investigation on the rheology of fault rocks dissertation, Basel Universität, Basel.
Perrillat, J. P., I. Daniel, J. M. Lardeaux, and H. Cardon (2003), Kinetics of the coesite-quartz transition: Application to the exhumation of ultrahigh-pressure rocks, *J. Petrol.*, *44*, 773–788, doi:10.1093/petrology/44.4.773.
Petrini, K., and Y. Podladchikov (2000), Lithospheric pressure-depth relationships in compressive regions of thickened crust, *J. Metamorph. Geol.*, *18*, 67–77, doi:10.1046/j.1525-1314.2000.00240.x.
Porter, D. A., and K. E. Easterling (1992), *Phase Transformation in Metals and Alloys*, pp. 514, Chapman and Hall, London.
Reuber, G., B. J. P. Kaus, S. M. Schmalholz, and R. W. White (2016), Nonlithostatic pressure during subduction and collision and the formation of (ultra)high-pressure rocks, *Geology*, *44*, 343–346, doi:10.1130/G37595.1.
Renner, J. (1996), Experimentelle Untersuchungen zur Rheologie von Coesit dissertation, Ruhr-Universität, Bochum.
Renner, J., B. Stöckhert, A. Zerbian, K. Röller, and F. Rummel (2001), An experimental study into the rheology of synthetic polycrystalline coesite aggregates, *J. Geophys. Res.*, *106*, 19,411–19,429, doi:10.1029/2001JB000431.
Robin, P. F. (1978), Pressure solution at grain-to-grain contacts, *Geochim. Cosmochim. Acta*, *42*, 1383–1389.
Rowe, C. D., and W. A. Griffith (2015), Do faults preserve a record os seismic slip: A second opinion, *J. Struct. Geol.*, *78*, 1–26, doi:10.1016/j.jsg.2015.06.006.
Rubie, D. C., and A. B. Thompson (1985), Kinetics of metamorphic reactions at elevated temperatures and pressures: An appraisal of available experimental data, in *Metamorphic Reactions*, edited by A. B. Thompson and D. C. Rubie, pp. 27–79, Springer, doi:10.1007/978-1-4612-5066-1_2.
Schmalholz, S. M., and Y. Y. Podladchikov (2013), Tectonic overpressure in weak crustal-scale shear zones and implications for the exhumation of high-pressure rocks, *Geophys. Res. Lett.*, *40*, 1984–1988, doi:10.1002/grl.50417.
Schmalholz, S. M., and Y. Podladchikov (2014), Metamorphism under stress: The problem of relating minerals to depth, *Geology*, *42*, 733–734, doi:10.1130/focus0822014.1.
Schönbohm, D. (2003), Untersuchungen zur Kinetik der Coesit–Quarz Umwandlung unter in-situ Bedingungen mittels Synchrotronstrahlung sowie Analyse der Mikrostrukturen im Transformationsbereich mittels TEM, dissertation, Rheinische Friedrich-Wilhelms-Universität, Bonn.
Shimizu, I. (1992), Kinetics of pressure solution creep in quartz: Theoretical considerations, *Tectonophysics*, *245*, 121–134.
Smith, D. C. (1984), Coesite in clinopyroxene in the Caledonides and its implications for geodynamics, *Nature*, *310*, 641–644, doi:10.1038/310641a0.
Stünitz, H. (1998), Syndeformational recrystallization – dynamic or compositionally induced?, *Contrib. Mineral. Petrol.*, *131*, 219–236, doi:10.1007/s004100050390.
Stüwe, K., and M. Sandiford (1994), Contributions of deviatoric stresses to metamorphic P-T paths: An example appropriate to low-P, high-T metamorphism, *J. Metamorph. Geol.*, *12*, 445–454, doi:10.1111/j.1525-1314.1994.tb00034.x.
Su, W., S. Liu, D. Xu, W. Wang, B. Yao, X. Liu, Z. Liu, and Z. Zhong (2006), Effects of local mechanical collision with shear stress on the phase transformation from α-quartz to coesite induced by high static pressure, *Phys. Rev.*, *73*, 144110, doi:10.1103/PhysRevB.73.144110.
Sun, N. X., X. D. Liu, and K. Lu (1996), An explanation to the anomalous Avrami exponent, *Scr. Mater.*, *34*, 1201–1207, doi:10.1016/1359-6462(95)00657-5.
Tajčmanová, L., J. Vrijmoed, and E. Moulas (2015), Grain-scale pressure variations in metamorphic rocks: Implications for the interpretation of petrographic observations, *Lithos*, *216–216*, 338–351, doi:10.1016/j.lithos.2015.01.006.
Tarantola, A., L. W. Diamond, H. Stünitz, A. Thust, and M. Pec (2012), Modification of fluid inclusions in quartz by deviatoric stress. III: Influence of principal stresses on inclusion density and orientation, *Contrib. Mineral. Petrol.*, *164*, 537–550, doi:10.1007/s00410-012-0749-1.
Wheeler, J. (2014), Dramatic effects of stress on metamorphic reactions, *Geology*, *42*, 647–650, doi:10.1130/G35718.1.
Zhou, Y., C. He, J. Song, S. Ma, and J. Ma (2005), An experiment study of quartz-coesite transition at differential stress, *Chin. Sci. Bull.*, *50*, 446–451, doi:10.1360/982004-234.
Zinn, P. (1996), Die Hochdrucksynthese von Coesit und die experimentelle Bestimmung seiner Stabilität als Funktion des Verzwilligungsgrades sowie Untersuchung zur Kinetik der Phasentransformation, dissertation, Justus-Liebig-Universität, Giessen.